Composite Structures 228 (2019) 111316

Contents lists available at ScienceDirect

Composite Structures

journal homepage: www.elsevier.com/locate/compstruct

An analytical model for wood composite sandwich beams with a biaxial corrugated core under bending

Mostafa Mohammadabadi[a], Vikram Yadama[b,*], Lloyd Smith[c]

[a] Material Science and Engineering Program and Composite Materials and Engineering Center, Washington State University, Pullman, WA 99164, USA
[b] Department of Civil and Environmental Engineering and Composite Materials and Engineering Center, Washington State University, Pullman, WA 99164, USA
[c] Department of Mechanical and Materials Engineering, Washington State University, Pullman, WA 99164, USA

ARTICLE INFO

Keywords:
Sandwich beam
Biaxial corrugated core
Analytical model
High-order sandwich panel theory
Homogenization method
Effective properties

ABSTRACT

In this study, an analytical model to evaluate the bending behavior of wood-based sandwich panels with a biaxial corrugated core was developed. A homogenization method was adopted to replace the geometry of the core with a homogeneous medium. Considering the deformation of the core under pure tension, compression, and shear, the properties of the homogenized core were computed. A high-order sandwich panel theory, that takes into account the deformation of the sandwich beam through the thickness, was applied to derive the governing equations. Fourier series expansions were used to solve the governing equations for a simply supported sandwich beam. The analytical results for sandwich beams with two different geometries were compared to finite element predictions and experimental results. The analytical model differed by 0.5–1.9% from the finite element model, and 1.6–7.8% with experiment.

1. Introduction

Sandwich structures are widely used in aerospace, automotive, civil, and marine industries due to their high strength/stiffness-to-weight ratio, and have been evaluated experimentally and numerically [1–6]. However, the development of an analytical model for sandwich structure with a complex core geometry such as honeycomb and corrugated cores is difficult because of the variation in the geometry of the cores [7]. One of the earliest analytical studies on sandwich panels was performed by Libove and Batdorf [8] to develop a small deflection theory for elastic behavior of sandwich panels with either homogenous or non-homogenous cores. He et al. [7] presented a semi-analytical method for the bending behavior of a corrugated core, honeycomb core and X core sandwich structures. They modelled the facesheets as plates and the core sheet as a beam, so that the sandwich panels were analyzed as a composite structure of plates and beams. Subsequently, classical sandwich plate theory, based on the geometry of the core along with minimum potential energy, was applied to derive the governing equations. Unfortunately, these analytical models cannot be applied for sandwich structures with biaxially corrugated cores, thus requiring the development of a new model.

Homogenization theory substitutes a heterogeneous structure with an equivalent homogeneous material, and can overcome the complexity of the core geometry [9]. The effective elastic constants of the equivalent homogeneous structure can be obtained using the homogenization method [10]. Libove and Hubka [11] presented formulas for evaluating the effective elastic constants of a corrugated core sandwich panel. These elastic constants, expressed in terms of the cross sectional area and moment of inertia of the actual geometry of the core, can be combined with general sandwich-plate theories to evaluate the behavior of the corrugated core sandwich structure. Chang et al. [12] used the formulas developed by Libove and Hubka [11] to obtain the effective properties of a corrugated core sandwich structure. Subsequently, they used the Mindlin–Reissner plate theory to investigate the linear bending behavior of a corrugated core sandwich structure. Others [13–15] have also computed core effective properties using the geometry of the core, where a known function describing the corrugation shape of the core was used to calculate the effective properties. For complicated core geometries, such as biaxial corrugated core sandwich beams, however, these approaches of finding effective properties are not valid.

For a corrugated core sandwich structure in which the core is also a sandwich member, Kazemahvazi et al. [16] proposed an analytical model using effective properties that are calculated from tensile, compressive, bending and shear deformations of elements comprising the core structure. Frostig et al. [17] developed a new theory for sandwich panels with a flexible core known as high-order sandwich panel theory (HSAPT). Unlike the most theories for sandwich structures that neglect

* Corresponding author.
E-mail address: vyadama@wsu.edu (V. Yadama).

https://doi.org/10.1016/j.compstruct.2019.111316
Received 13 May 2019; Accepted 16 August 2019
Available online 23 August 2019
0263-8223/ © 2019 Elsevier Ltd. All rights reserved.

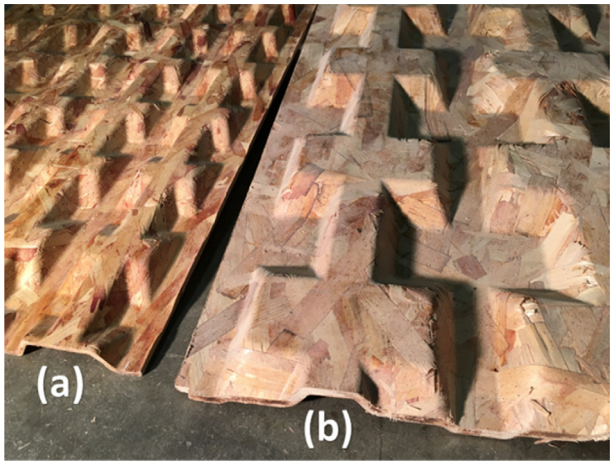

Fig. 1. Wood-based biaxial corrugated cores (a) Core A (b) Core B.

the deformation through the thickness direction, HSAPT defines a second-order polynomial function as a through thickness displacement field. Many researchers have used this theory for linear and nonlinear analysis of sandwich structures [18–22]. However, this theory has not been used for sandwich panels with a corrugated core geometry.

Voth et al. [23] developed a wood-based sandwich structure with a biaxial corrugated core [20]. Experimental studies have revealed this type of sandwich structure to have improved bending response in the transverse directions as well as longitudinal direction [24,25]. To the authors' knowledge, no analytical model has been developed for sandwich structures with a biaxial core. In this study an analytical model was developed to describe the bending behavior of wood-strand sandwich beams with two different biaxial corrugated cores as shown in Fig. 1. The analytical bending response for two core geometries was compared with experiment and a finite element model.

2. Materials and fabrication process

The core and facesheets of the sandwich panels were fabricated from thin strands with an average thickness of 0.38 mm. Strands were produced from small diameter ponderosa pine and lodgepole pine logs. Strands were resinated with 8% phenol formaldehyde resin in a drum blender. A mat or preform of resinated strands oriented parallel to the longitudinal direction as shown in Fig. 2a was formed. The unidirectional wood-strand mat was hot pressed at 160 °C for 6 min to fabricate the 6.35 mm thick facesheets. The top and bottom facesheet thickness was designated h_t and h_b, respectively. The biaxial corrugated cores were made using matched die molds with a process similar to the facesheets. Sandwich panels were formed by bonding two flat layers to a corrugated core using a polyurethane adhesive (LOCTITE HB X452 PURBOND, Henkel) at room temperature.

A unit cell (UC) of the corrugated structure is highlighted in Fig. 2a. The UC dimensions for two configurations are given in Fig. 2b and the associated table.

Engineering elastic constants were obtained from tension, compression, and shear tests following ASTM guidelines [26] of small coupons cut from flat layers and are presented in Table 1. These elastic constants are given in a local coordinate system, 1-2-3, shown in Fig. 2b, where the 1-axis is parallel to the wood fibers. Because of the complicated core geometry, a local coordinate system was defined for each core face. Faces with the same color in Fig. 2b represent the same local coordinate system. A global coordinate system, x-y-z, is shown in Fig. 2a. As the fiber orientation in individual strands varies in the width direction with respect to an idealized orthotropic material axes and the layers are a conglomeration of wood strands oriented uniaxially, transverse isotropy was assumed for the material properties of both face and core layers given in Table 1 [28].

3. Finite element model

SolidWorks software (Education Edition) was used as a preprocessor to simulate and generate the complex geometry of the corrugated core. Then, finite element software (Abaqus, version 6.14-1) was used as a solver to describe the bending behavior of the sandwich beams with biaxial corrugated cores. Shell elements were used to model the core layer, whereas the facesheets were modeled using solid elements. The nodes in the contact area between the bottom facesheet and the support were constrained in the z-direction. As observed with experiment, all other nodes were unconstrained.

4. High-order sandwich panel theory

Due to the corrugated geometry of the core and the resulting flexibility [11,27], deformation in the z-direction of the sandwich beams, caused by bending loads, can be important. Through the thickness deformation leads to a change in cross section as shown in Fig. 3. Notably, cross section deformation in Fig. 3b were captured at the free edge of the overhang. In the following, a high-order sandwich panel theory (HSAPT) was used to describe through thickness core deformation [17].

The displacement field for HSAPT is defined by third- and second-order polynomial functions [22] through the length and thickness of the core, respectively, as

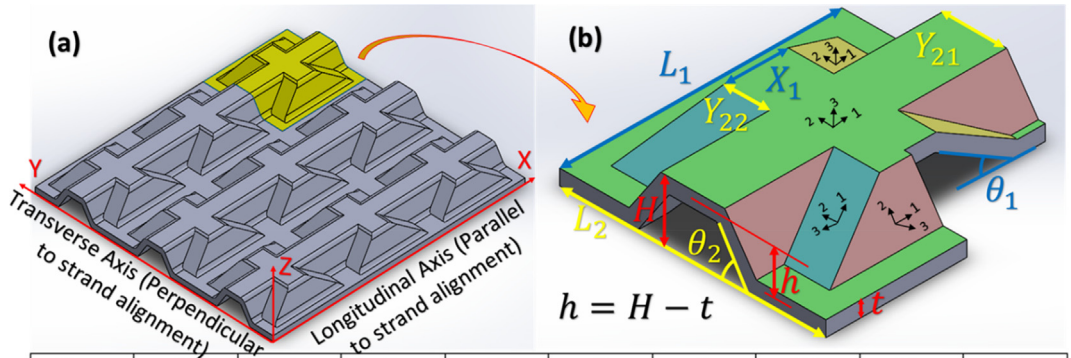

Core	H	t	L_1	L_2	θ_1	θ_2	X_1	Y_{21}	Y_{22}
A	25	6.4	114	108	30	56	23	19	19
B	35	7.6	203	203	40	56	63	30	48

Fig. 2. Schematic of a biaxial corrugated core (a) longitudinal and transverse directions along with highlighted unit cell and (b) dimensions of unit cell (mm).

Table 1
Material Properties of wood composite material.

E_1 (GPa)	E_2 (GPa)	E_3 (GPa)	υ_{12}	υ_{13}	υ_{23}	G_{12} (GPa)	G_{13} (GPa)	G_{23} (GPa)
9.80	1.71	1.71	0.358	0.358	0.2	2.56	2.56	0.71

$$\begin{cases} u^c(\mathrm{x_c}, \mathrm{z_c}) = u_0^c(\mathrm{x}) + z_c\varphi_0^c(\mathrm{x}) + z_c^2 u_1^c(\mathrm{x}) + z_c^3 u_2^c(\mathrm{x}) \\ w^c(\mathrm{x_c}, \mathrm{z_c}) = w_0^c(\mathrm{x}) + z_c w_1^c(\mathrm{x}) + z_c^2 w_2^c(\mathrm{x}) \end{cases} \tag{1}$$

where c refers to the core, $w_0(x)$, $u_0(x)$ and $\varphi_0(x)$ are deflection in the thickness direction (i.e., z-direction), the axial displacement, and angle of rotation of cross section about the y-axis with respect to the thickness direction, respectively. The coefficients of $w_1(x)$, $w_2(x)$, $u_1(x)$, and $u_2(x)$ are unknown functions that are obtained using the compatibility equations at the interface layer of the core and facesheets. The compatibility equations are given as

$$\begin{aligned} &w^c\left(\mathrm{x}, -\tfrac{H}{2}\right) = w^t\left(\mathrm{x}, \tfrac{h_t}{2}\right),\ u^c\left(\mathrm{x}, -\tfrac{H}{2}\right) = u^t\left(\mathrm{x}, \tfrac{h_t}{2}\right) \\ &w^c\left(\mathrm{x}, \tfrac{H}{2}\right) = w^b\left(\mathrm{x}, -\tfrac{h_b}{2}\right),\ u^c\left(\mathrm{x}, \tfrac{H}{2}\right) = u^b\left(\mathrm{x}, -\tfrac{h_b}{2}\right) \end{aligned} \tag{2}$$

where t and b indicate top and bottom facesheets, and H is the height of the corrugated core. The displacement field of the classical beam theory that is used to evaluate the facesheets is expressed as

$$\begin{cases} u^f(\mathrm{x_f}, \mathrm{z_f}) = u_0^f(\mathrm{x}) - z_f \frac{\partial w_0^f}{\partial x} \\ w^f(\mathrm{x_f}, \mathrm{z_f}) = w_0^f \end{cases} \tag{3}$$

where f (superscripts and subscripts) refers to the top (t) or bottom (b) facesheets. Dimensions of the bending specimen with local coordinate systems are shown in Fig. 4. The unknown displacement functions, $w_1(x)$, $w_2(x)$, $u_1(x)$, and $u_2(x)$ are determined by substituting Eqs. (1) and (3) into Eq. (2). The core displacement field in Eq. (1) becomes

$$\begin{cases} u^c(x, z) = u_0^c(x) + z_c\phi_0^c(x) \\ \quad + z_c^2\left[\frac{2}{H^2}\left(u_0^t(\mathrm{x}) - \frac{h_t}{2}\frac{\partial w_0^t}{\partial x} + u_0^b(\mathrm{x}) + \frac{h_b}{2}\frac{\partial w_0^b}{\partial x} - 2u_0^c(\mathrm{x})\right)\right] \\ \quad + z_c^3\left[\frac{4}{H^3}\left(-u_0^t(\mathrm{x}) + \frac{h_t}{2}\frac{\partial w_0^t}{\partial x} + u_0^b(\mathrm{x}) + \frac{h_b}{2}\frac{\partial w_0^b}{\partial x} - c\phi_0^c(\mathrm{x})\right)\right] \\ w^c(\mathrm{x}, \mathrm{z}) = w_0^c(\mathrm{x}) + z_c\left[\frac{1}{H}(w_0^b(\mathrm{x}) - w_0^t(\mathrm{x}))\right] \\ \quad + z_c^2\left[\frac{2}{H^2}(w_0^t(\mathrm{x}) + w_0^b(\mathrm{x}) - 2w_0^c(\mathrm{x}))\right] \end{cases} \tag{4}$$

Using Eq. (4) for the core and Eq. (3) for the facesheets, the components of the strain tensor can be computed in terms of displacement, from which we obtain

$$\begin{Bmatrix} \sigma_{xx}^{t,c,b} \\ \sigma_{zz}^{t,c,b} \\ \sigma_{xz}^{t,c,b} \end{Bmatrix} = \begin{bmatrix} Q_{11} & Q_{13} & 0 \\ Q_{31} & Q_{33} & 0 \\ 0 & 0 & Q_{55} \end{bmatrix}^{t,c,b} \begin{Bmatrix} \varepsilon_{xx}^{t,c,b} \\ \varepsilon_{zz}^{t,c,b} \\ \gamma_{xz}^{t,c,b} \end{Bmatrix} \tag{5}$$

The components of stiffness matrix are described in [29]. Because classical beam theory is used for the facesheets, we have $\varepsilon_{zz}^{t,b} = \gamma_{xz}^{t,b} = 0$. The governing equations and boundary conditions are derived using the variational form of the principle of minimum potential energy as [30]

$$\delta\Pi = \delta U - \delta W = 0 \tag{6}$$

The variation of strain energy is

$$\delta U = \int_0^L \left[\sum_{k=t,c,b} \int ((\sigma^k)^T : \delta\varepsilon) dA_k\right] dx \tag{7}$$

where L and A are respectively span length and cross section of the components of the sandwich beams as shown in Fig. 4. The first variation of virtual work done by external forces, is

$$\delta W = \int_0^L [f_x\delta u + f_z\delta w + m_{xy}\delta\varphi] dx + \sum_{l=1}^{n} [\bar{N}\delta u + \bar{V}\delta w + \bar{M}\delta\varphi]\delta_d(x - x_l) \tag{8}$$

In which f_x and f_z are the x- and z-components of body forces, respectively, and m_{xy} is the y-component of body moment. Also $\bar{N}$, $\bar{V}$, and $\bar{M}$ are, respectively, the applied axial force, transverse shear force, bending moments at point $x = x_l$. The number of concentrated loads and moments is identified by n, while $\delta_d(x - x_l)$ is the Dirac delta function that is used to define the position of these concentrated loads on the beam. Substituting Eqs. (7) and (8) in Eq. (6) and applying the fundamental lemma of the calculus of variation result in governing equations and boundary conditions.

5. Homogenization method

Computing Eq. (7) is cumbersome because the geometry of the core results in a varying cross section along its length. A homogenization method was used to overcome this difficulty. The corrugated geometry of the core was replaced with a continuous core that has a constant cross section. The effective properties of the homogenized core are established using simple constitutive and linear beam equations as

$$\delta = \frac{F_{T\&C}L}{AE},\ \delta = \frac{F_S L}{GA},\ \delta = \frac{F_B L^3}{3EI} \tag{9}$$

where $F_{T\&C}$, F_S, and F_B are tensile or compression load, shear load, and bending load, E and G are material properties, A and I are area and moment of inertia of the beam cross section.

5.1. Effective Young's modulus in the x-direction, E_x^{eff}

Due to symmetry, the tensile response of one half of a UC of the

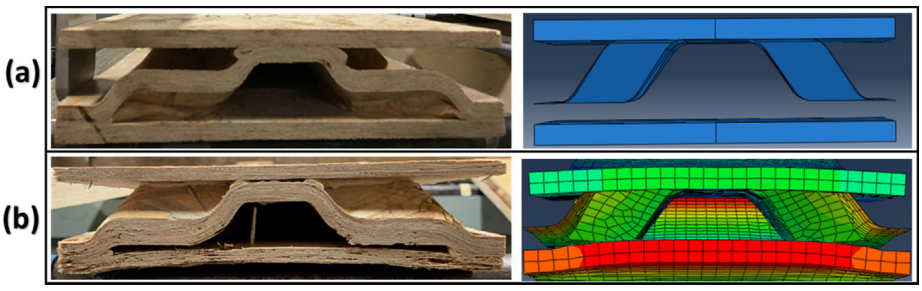

Fig. 3. Deformation through the thickness due to flexibility of the core. Cross section (a) before and (b) after applying bending load.

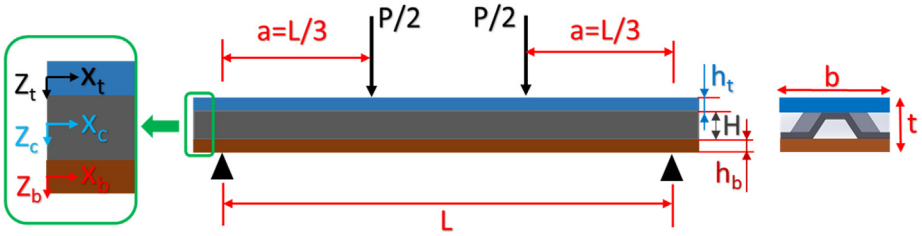

Fig. 4. Schematic view of sandwich beam under bending load.

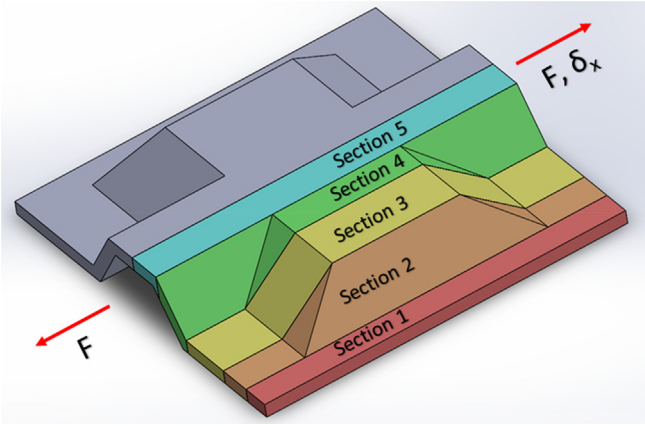

Fig. 5. UC submitted to tensile loading to obtain effective E_1.

corrugated core was considered as shown in Fig. 5. The half UC was divided into five sections, also shown in Fig. 5. Since sections 1 and 5 are without any corrugation, the tensile load is given as

$$F_i = \frac{AE}{L}\delta_x = \frac{\left(\frac{Y_{21}}{2}t\right)E_1}{L_1}\delta_x \; i = 1, 5 \tag{10}$$

where Y_{21}, L_1, and t are core dimensions shown in Fig. 2, and E_1 is the longitudinal Young's modulus of the wood composite material given in Table 1. For the sections 2, 3, and 4, a thin element of width dy was considered as shown in Fig. 6. Parametric equations describing the dimensions of these sections are given in Table 2. The cross sectional area and moment of inertial for different parts (a, b, and c) of the thin element shown in Fig. 6 are indicated by A and I with corresponding subscripts and also given in Table 2.

Since the tensile load on each small element (dF_i) is applied eccentrically, a bending moment (dM_i) is created on the element. The offset distance, h_i'', for this eccentric load from the centroid is given as

$$h_i'' = \frac{\sum V_i h_i}{\sum V_i} = \frac{2L_{bi}A_{bi}(h_i'/2) + L_{ci}A_{ci}(h_i')}{2L_{ai}A_{ai} + 2L_{bi}A_{bi} + L_{ci}A_{ci}} \tag{11}$$

where V_i and h_i are the volume and moment arm for each element, respectively. Considering the relations given in Eq. (9) and geometric parameters given in Table 2, the relation between eccentric load that acts on each element and specified displacement of δ_x can be expressed as

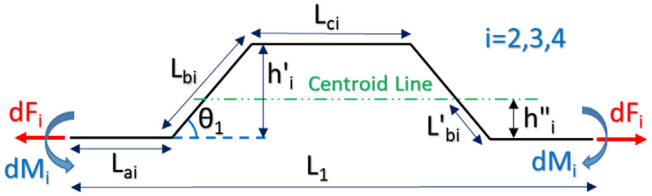

Fig. 6. Schematic view of thin elements cut from sections 2, 3, and 4 shown in Fig. 5.

Table 2
Geometrical parameters specified in Fig. 6 for Sections 2–4.

Section	Geometric parameters
2	$L_{a2} = \frac{X_1}{2}$, $L_{b2} = \frac{h_2'}{sin\theta_1}$, $L_{c2} = L_1 - 2L_{a2} - 2L_{a2}cos\theta_1$, $h_2' = ytan\theta_2$
	$A_{a2} = A_{b2} = tdy$, $A_{c2} = \frac{t}{cos\theta_2}dy$, $I_{b2} = \frac{t^3}{12}dy$, $y \in [0,\ h/tan\theta_2]$
3	$L_{a3} = \frac{X_1}{2}$, $L_b = h_3'/sin\theta_1$, $L_{c3} = X_1$, $h_3' = h$
	$A_{a3} = A_{b3} = A_{c3} = tdy$, $I_{b3} = \frac{t^3}{12}dy$, $y \in \left[0,\ Y_{22} - \frac{h}{tan\theta_2}\right]$
4	$L_{a4} = \frac{X_1}{2} + \frac{ytan\theta_2}{tan\theta_1}$, $L_{b4} = \frac{h_4'}{sin\theta_1}$, $L_{c4} = X_1$, $h_4' = h - ytan\theta_2$
	$A_{a4} = \frac{t}{cos\theta_2}dy$, $A_{b4} = A_{c4} = tdy$, $I_{b4} = \frac{t^3}{12}dy$, $y \in [0,\ h/tan\theta_2]$

$$dF_i = \frac{\delta_x}{\left[\frac{2L_{ai}}{A_{ai}E_1} + \frac{2(L_{bi}'^3 + (L_{bi} - L_{bi}')^3)(sin\theta_1)^2}{3E_1I_{bi}} + \frac{2L_{bi}(sin\theta_1)^2}{G_{12}A_{bi}} + \frac{2L_{bi}(cos\theta_1)^2}{A_{bi}E_1} + \frac{L_{ci}}{A_{ci}E_1}\right]}i$$
$$= 2, 3, 4 \tag{12}$$

Integrating dF_i over the width gives the tensile load for sections 2, 3, and 4. The effective longitudinal Young's modulus of the core is now defined as

$$E_x^{eff} = \frac{2L_1(F_1 + F_2 + F_3 + F_4 + F_5)}{HL_2}\delta_x \tag{13}$$

5.2. Effective through thickness modulus, E_z^{eff}

Due to symmetry, one quarter of the UC was considered for through thickness compressive response as shown in Fig. 7. The through thickness compressive load creates F_1 and F_2, and F_{1h} and F_{2h}, as shown in Fig. 7. Since $E_1 \gg E_2$, the horizontal deformation in the longitudinal direction caused by F_{2h} is small and was neglected.

Applying the principle of superposition, δ_z can be expressed in terms of deformation in the inclined walls (δ') and deformation in the horizontal parts (δ''), as depicted in Fig. 8.

Because of the continuity and symmetrical geometry of the UC, all inclined walls must have the same δ_s. Thus, the compression loads in

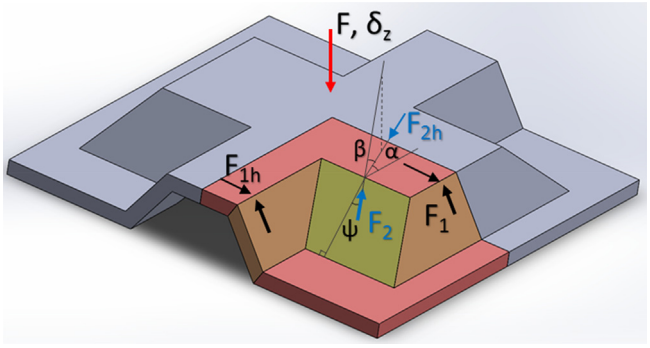

Fig. 7. UC submitted to compression loading to obtain effective E_3.

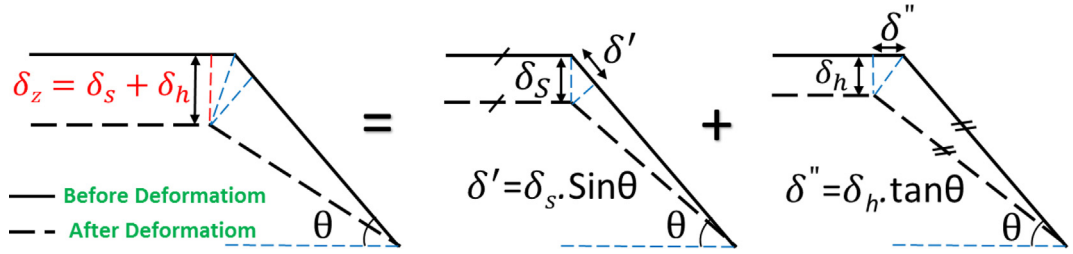

Fig. 8. Components of the transverse deflection in the inclined and horizontal sections of the core due to transverse compression loading as shown in Fig. 7.

the inclined walls, F_1 and F_2, can be found using

$$F_1 = \frac{L_1 t E_2}{2h}\delta_s (sin\theta_2)^2,\ F_2 = \frac{Y_{22} t E_1^{'}}{h}\delta_s (sin\beta)^2,\ F_1 sin\theta_2 + F_2 sin\beta = F \tag{14}$$

where $E_1^{'}$ is the modulus of the wood composite material in the direction parallel to F_2 shown in Fig. 7, expressed as

$$E_1^{'} = \left[\frac{m^4}{E_1} + \frac{n^4}{E_2} - \frac{2m^2n^2\upsilon_{12}}{E_1} + \frac{m^2n^2}{G_{12}}\right]^{-1} m = cos\psi,\ n = sin\psi$$

$$\alpha = tan^{-1}\left(\frac{tan\theta_1}{tan\theta_2}\right),\ \beta = tan^{-1}(tan\theta_2 sin\alpha),\ \psi = sin^{-1}(sin\alpha cos\beta) \tag{15}$$

Considering Eq. (14), δ_s is given as

$$\delta_s = aF,\ a = \frac{2h}{[L_1 t E_2 (sin\theta_2)^3 + 2Y_{22} t E_1^{'}(sin\beta)^3]} \tag{16}$$

Substituting Eq. (16) in Eq. (14), the compression loads in the inclined walls, F_1 and F_2, can be described in terms of the total compression load applied to the UC as

$$F_1 = bF,\ b = \frac{L_1 t E_2 (sin\theta_2)^2}{[L_1 t E_2 (sin\theta_2)^3 + 2Y_{22} t E_1^{'}(sin\beta)^3]}$$
$$F_2 = cF,\ c = \frac{2Y_{22} t E_1^{'}(sin\beta)^2}{[L_1 t E_2 (sin\theta_2)^3 + 2Y_{22} t E_1^{'}(sin\beta)^3]} \tag{17}$$

Now, loads F_{1h} and F_{2h}, can be found from F_1 and F_2, given in Eq. (17). Then, δ_h can be obtained from

$$\delta_h = eF,\ e = \frac{1}{tan\theta_2}\left[\frac{(bcos\theta_2 + 2csin\alpha cos\beta)\left(Y_{22} + \frac{Y_{21}}{2}\right)}{X_1 t E_2} + \frac{(bcos\theta_2)\left(\frac{Y_{21}}{2}\right)}{(L_1 - X_1) t E_2}\right] \tag{18}$$

The effective modulus of the core through the thickness becomes

$$E_z^{eff} = \frac{4FH}{L_1 L_2 (\delta_s + \delta_h)} = \frac{4H}{(L_1 L_2)(a + e)} \tag{19}$$

5.3. Effective shear modulus in the x-z plane, G_{xz}^{eff}

Because of the complicated geometry of the core, it is difficult to derive an effective shear modulus using the UC deformation and the simple equations given in Eq. (9). To address this issue, the finite element method was used to find an equivalent and simplified geometry that represents the shear behavior of the real geometry. The deformation of this simplified geometry under shear load was used to find the effective shear modulus.

When a UC of the corrugated core is submitted to shear loading, the inclined walls, which undergo shear, tensile, and compressive deformations, play an important role to carry the load. Thus, the dimensions of inclined walls are important to find a simplified geometry that has a similar shear behavior to the real configuration. A UC of the actual and simplified geometries of the corrugated core are shown in Fig. 9a and b, respectively. As can be seen, the height and wall thickness of the simplified geometry in Fig. 9b have been increased compared to the actual geometry shown in Fig. 9a to retain the length of the inclined walls carrying the shear load. In the finite element model, both the actual and simplified geometries were submitted to the same shear forces. Comparison between the shear modulus, G, of the actual and simplified geometries revealed a 0.26% and 0.22% difference for cores A and B, respectively. Considering this strong agreement, the relations in Eq. (9) were applied to this new simplified geometry to derive the effective shear modulus in the x-z plane.

For a simplified UC (Fig. 9b) loaded in shear, the red sections shown in Fig. 10a were subjected to shear, while the green were loaded in bending as shown in Fig. 10b. The shear displacement (δ_{xz}) and shear force (F_1) acting on the vertical walls are related by

$$F_1 = \frac{G_{12} t_N (L_1 + 2t_N)}{H^{'}}\delta_{xz} \tag{20}$$

where t_N, H', and L_1 are core parameters shown in Fig. 9.

For those vertical walls with bending deformation (Fig. 10b), the shear load (F_2) can be defined in terms of shear displacement (δ_{xz}) as

$$F_2 = \frac{(Y_{22} - t_N)}{\left[\frac{4}{E_1}\left(\frac{H^{'}}{t_N}\right)^3 + \frac{1}{G_{13}}\left(\frac{H^{'}}{t_N}\right)\right]}\delta_{xz} \tag{21}$$

The effective shear modulus in the x-z plane is now expressed as

$$G_{xz}^{eff} = \frac{H^{'}(2F_1 + 4F_2)}{(L_1 L_2)\delta_{xz}} = \frac{H^{'}}{(L_1 L_2)}\left[\frac{2Gt_N(L_1 + 2t_N)}{H^{'}} + 4\left(\frac{(Y_{22} - t_N)}{\left[\frac{4}{E_1}\left(\frac{H^{'}}{t_N}\right)^3 + \frac{1}{G_{13}}\left(\frac{H^{'}}{t_N}\right)\right]}\right)\right] \tag{22}$$

6. Solution method

In this study, the bending behavior of simply supported sandwich beams with two different corrugated core geometries, as shown in Fig. 1, was investigated. Fourier series expansions, which satisfy the boundary conditions of simply supported beams and plates, were used to solve the governing equations of beams and plates. The expansions for generalized displacements $u_0(x)$ and $w_0(x)$ and rotation $\varphi_0(x)$ are [22,31]

$$u_0^{t,c,b} = \sum_{n=1}^{\infty} U_n^{t,c,b}\cos\left(\frac{n\pi x}{L}\right),\ w_0^{t,c,b} = \sum_{n=1}^{\infty} W_n^{t,c,b}\sin\left(\frac{n\pi x}{L}\right),\ \varphi_0^c = \sum_{n=1}^{\infty}\phi_n^c\cos\left(\frac{n\pi x}{L}\right) \tag{23}$$

where U_n, W_n, and ϕ_n are the Fourier coefficients. After solving the governing equations and obtaining the deflection at mid-span of the beam, the bending stiffness for sandwich beams under four point bending is expressed as

$$D = \frac{Pa}{48\Delta}(3L^2 - 4a^2) \overset{a=\frac{L}{3}, m=\frac{P}{\Delta}}{\rightarrow} D = \frac{23mL^3}{1296} \tag{24}$$

where P, Δ, L, and m are the bending load, deflection at mid-span,

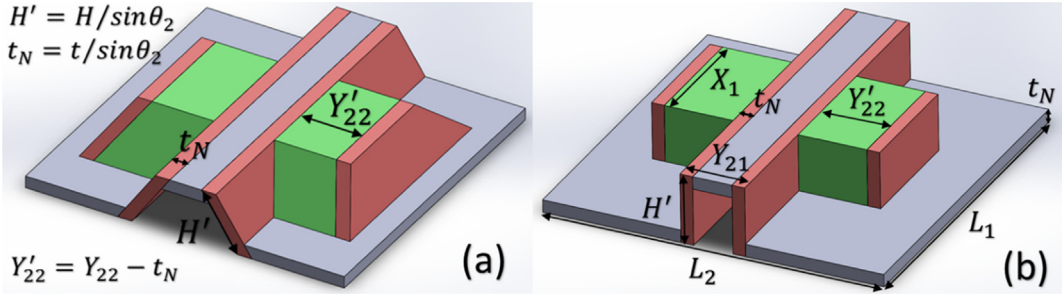

Fig. 9. A UC of the corrugated core (a) actual geometry (b) simplified geometry with similar shear behavior.

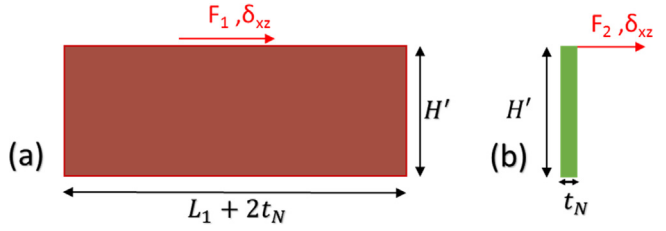

Fig. 10. Vertical walls of simplified UC (shown in Fig. 9b) subjected to shear loading undergo (a) shear deformation and (b) tensile deformation.

Table 3
Dimensions of sandwich beams used for bending test (mm).

Core Type	Specimen Configuration	Width b	Span length L	Thickness $t = h_t + H + h_b$	Slenderness ratio L/t
A	Short and wide	216	969	38	25.5
A	Long and narrow	108	1938	38	51
B	Short and wide	406	1219	47.6	25.6
B	Long and narrow	203	2437	47.6	51.2

span length, and slope of the load–deflection curve, respectively. The constant "a" is the distance between the support and loading point as shown in Fig. 4.

7. Results and discussions

Sandwich beams were submitted to four-point bending test as shown in Fig. 4. After obtaining the beam deflection at mid-span, the bending stiffness was computed using Eq. (24). For the analytical model, the effective properties obtained from the homogenization method were used where the Poisson effect was not considered [7]. In this section, analytical, FE, and experimental bending stiffness of sandwich beams with both core A and B are compared. Notably, two different span lengths were chosen to evaluate the bending behavior of sandwich beams: 1) long and narrow (with 1 UC wide), and 2) short and wide (2 UC wide). The specimens' dimensions are given in Table 3.

Since the mold to fabricate Core A was only 787 mm long, comparison with experiment was not possible for the sandwich beams with Core A. Comparison between the analytical bending stiffness of these sandwich beams with those of the FE model is presented in Fig. 11a. Predictions of bending stiffness based on the analytical model is 1.9% higher than FE for a slenderness ratio of 25.5, short and wide specimens. As the slenderness ratio doubled, i.e. long and narrow specimens, the difference between the analytical and FE bending stiffness was approximately −0.5%. The negative difference indicates that the analytical results fall on the conservative side of the FE predictions. Since, the analytical model was developed for sandwich beams, an increase in specimen length (from 972 mm to 1943 mm) accompanied with a decrease in width (from 216 mm to 108 mm) improved the agreement between the analytical and FE models.

The same slenderness ratios for core A was used to determine the span length of sandwich beams with Core B. Comparison between the analytical bending stiffness of these sandwich beams with those of FE and experimental results is presented in Fig. 11b. For Core B, the slenderness ratio of 25.6, i.e. short and wide specimens, yielded an analytical bending stiffness that was 0.85% to 7.8% higher than those of FE and experimental bending stiffness values. For beams with a longer span (2437 mm) and greater slenderness ratio (51.2), the difference in the results between the analytical and FE and experimental bending stiffness was −2.8% and −1.6%. The analytical model was developed for beams and therefore does not capture deformation along the width of the specimen, thus potentially contributing to differences between the theoretical and the experimental results in addition to the slenderness ratio. In addition, the complex geometry of the core, the nonhomogeneous wood composite material, and the inherent variations in material properties also contribute to these differences between the analytical and the experimental bending stiffness of sandwich beams, especially with small slenderness ratio when shear deformations are significant.

Comparison of the bending stiffness showed that the analytical model can efficiently estimate the effective elastic properties of the

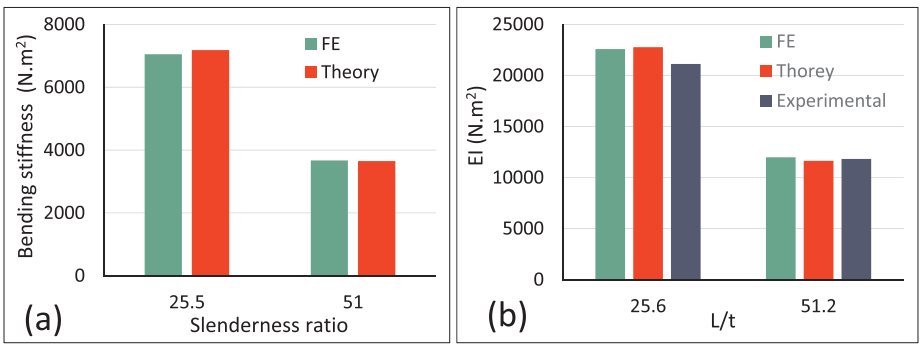

Fig. 11. Comparison between analytical, FE, and experimental bending stiffness of sandwich beam with (a) Core A and (b) Core B.

Table 4
Comparison of some properties of the homogenized and corrugated cores.

Core		E_1 (GPa)	E_3 (GPa)	G_{13} (GPa)	A* (cm^2)	I* (cm^4)	E_1.A* (GPa.cm^2)	E_1.I* (GPa.cm^4)
A	Homogenized	1.61	0.075	14.73	27.42	14.73	44.15	23.72
	Corrugated	9.80	1.71	5.23	8.35	5.23	81.83	51.25
B	Homogenized	1.21	0.046	72.13	70.97	72.13	85.87	87.28
	Corrugated	9.80	1.71	25.28	18.40	25.28	180.3	247.7

* For corrugated core, using SolidWorks, these properties were computed for numerous cross sections through the length and then, were averaged.

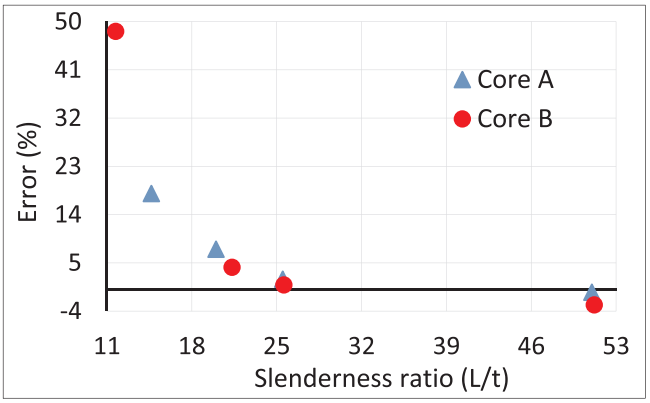

Fig. 12. Difference between analytical and FE bending stiffness of sandwich beam for different slenderness ratios.

homogenized core and bending behavior of the sandwich beams. Unlike some studies [13–15] that have used the actual geometry of the core to compute the effective properties, the analytical model developed in this study used a homogenization method to obtain the core effective properties. A comparison between the effective properties of the homogenized core and those of the actual corrugated core is presented in Table 4. The axial stiffness, *EA*, and bending stiffness, *EI*, of the core show a significant difference between the corrugated cores with the homogenized one. This difference reveals the importance of using the homogenized core instead of the actual core geometry to develop an analytical model. In fact, employing the actual geometry to develop an analytical model requires the actual material properties, area and moment of inertia, while the homogenization method also takes the deformation of the UC into account to derive the effective properties.

The results for sandwich beams with both Core A and B indicated that the analytical model shows a better agreement with FE and experimental results for long specimens compared to the short sandwich beams. In other words, the slenderness ratio of the sandwich beams can affect the accuracy of the analytical model. To evaluate this effect, difference between the bending stiffness obtained by the analytical model with those predicted by FE for different slenderness ratio is given in Fig. 12. The negative error shows that the analytical model predicts lower bending stiffness than the FE model and falls on the conservative side. This figure shows that for slenderness ratios lower than 20, the error in bending stiffness is more than 8%.

8. Conclusions

In this study, a high-order sandwich panel theory, that takes into account the deformation of the beam through the thickness, was used to derive the governing equations for predicting the elastic bending stiffness of wood strand sandwich beams with biaxial corrugated cores. A homogenization method was applied to replace the discrete geometry of the core with a homogeneous material to simplify the analysis of a beam with a complex core geometry. Using deformation of a UC under tension, compression, and shear loading along with a simple relation obtained from constitutive equations and a linear beam model, equations to determine the effective properties of the homogenized core were derived and used in a constitutive model. Comparison between the predicted bending stiffness using the analytical model and the FE model and experimental results revealed 0.5% to 7.8% difference. The analytical method was most effective for predicting the bending stiffness of long beams.

The analytical model developed in this study can be used to efficiently estimate the effective elastic properties and to understand how geometrical parameters affect the bending behavior of the sandwich beams with a biaxial corrugated core. The effect of these geometrical parameters on the bending stiffness can be used in design of new biaxial corrugated cores to achieve a higher bending stiffness.

Acknowledgement

The authors would like to thank CMMI, National Science Foundation for funding this research, grant # 1150316.

References

[1] Russo A, Zuccarello B. Experimental and numerical evaluation of the mechanical behaviour of GFRP sandwich panels. Compos Struct 2007;81(4):575–86.
[2] Mamalis AG, et al. On the crushing response of composite sandwich panels subjected to edgewise compression: experimental. Compos Struct 2005;71(2):246–57.
[3] Valdevit Lorenzo, et al. Structural performance of near-optimal sandwich panels with corrugated cores. Int J Solids Struct 2006;43(16):4888–905.
[4] Hou Shujuan, et al. Experimental and numerical studies on multi-layered corrugated sandwich panels under crushing loading. Compos Struct 2015;126:371–85.
[5] Biancolini ME. Evaluation of equivalent stiffness properties of corrugated board. Compos Struct 2005;69(3):322–8.
[6] Levent A, Alastair F Johnson, Bernd HK. Numerical modeling of honeycomb core crush behavior. Eng Fract Mech 2007.
[7] He Li, Cheng Yuan-Sheng, Liu Jun. Precise bending stress analysis of corrugated-core, honeycomb-core and X-core sandwich panels. Compos Struct 2012;94(5):1656–68.
[8] Libove, Charles, Batdorf SB. A general small-deflection theory for flat sandwich plates. No. NACA-899. NATIONAL AERONAUTICS AND SPACE ADMINISTRATION WASHINGTON DC; 1948.
[9] Buannic Natacha, Cartraud Patrice, Quesnel Tanguy. Homogenization of corrugated core sandwich panels. Compos Struct 2003;59(3):299–312.
[10] Bourgeois S, Cartraud P, Debordes O. Homogenization of periodic sandwiches. Mechanics of Sandwich Structures. Dordrecht: Springer; 1998. p. 131–8.
[11] Libove Charles, Hubka Ralph E. Elastic constants for corrugated-core sandwich plates. 1951.
[12] Chang Wan-Shu, et al. Bending behavior of corrugated-core sandwich plates. Compos Struct 2005;70(1):81–9.
[13] Aboura Zoheir, et al. Elastic behavior of corrugated cardboard: experiments and modeling. Compos Struct 2004;63(1):53–62.
[14] Magnucki Krzysztof, et al. Strength and buckling of sandwich beams with corrugated core. J Theor Appl Mech 2013;51(1):15–24.
[15] Cheon Young-Jo, Kim Hyun-Gyu. An equivalent plate model for corrugated-core sandwich panels. J Mech Sci Technol 2015;29(3):1217–23.
[16] Kazemahvazi Sohrab, Zenkert Dan. Corrugated all-composite sandwich structures. Part 1: modeling. Compos Sci Technol 2009;69(7-8):913–9.
[17] Frostig Y, et al. High-order theory for sandwich-beam behavior with transversely flexible core. J Eng Mech 1992;118(5):1026–43.
[18] Frostig Y. On stress concentration in the bending of sandwich beams with transversely flexible core. Compos Struct 1993;24(2):161–9.
[19] Bozhevolnaya Elena, Frostig Y. Nonlinear closed-form high-order analysis of curved sandwich panels. Compos Struct 1997;38(1-4):383–94.
[20] Sokolinsky Vladimir S, et al. Experimental and analytical study of nonlinear bending response of sandwich beams. Compos Struct 2003;60(2):219–29.
[21] Kim Jongman, Swanson Stephen R. Design of sandwich structures for concentrated loading. Compos Struct 2001;52(3-4):365–73.
[22] Dariushi Soheil, Sadighi Mojtaba. A new nonlinear high order theory for sandwich beams: an analytical and experimental investigation. Compos Struct 2014;108:779–88.
[23] Voth Christopher, et al. Design and evaluation of thin-walled hollow-core wood-

strand sandwich panels. J Renewable Mater 2015;3(3):234–43.
[24] Mohammadabadi Mostafa, Yadama Vikram, Geng Jian. Creep behavior of 3D core wood-strand sandwich panels. Holzforschung 2018;72(6):513–9.
[25] Mohammadabadi Mostafa, et al. Low-velocity impact response of wood-strand sandwich panels and their components. Holzforschung 2018;72(8):681–9.
[26] ASTM D1037. Standard test methods for evaluating properties of wood-base fiber and particle panel materials. West Conshohocken, PA: ASTM; 2006.
[27] Nordstrand Tomas, Carlsson Leif A, Allen Howard G. Transverse shear stiffness of structural core sandwich. Compos Struct 1994;27(3):317–29.
[28] Yadama Vikram, Wolcott Michael P, Smith Lloyd V. Elastic properties of wood-strand composites with undulating strands. Compos A Appl Sci Manuf 2006;37(3):385–92.
[29] Jones Robert M. Mechanics of composite materials. CRC press; 2014.
[30] Abadi M Mohammad, Daneshmehr AR. An investigation of modified couple stress theory in buckling analysis of micro composite laminated Euler-Bernoulli and Timoshenko beams. Int J Eng Sci 2014;75:40–53.
[31] Daneshmehr Ali Reza, Abadi Mostafa Mohammad, Rajabpoor Amir. Thermal effect on static bending, vibration and buckling of Reddy beam based on modified couple stress theory Trans Tech Publications Appl Mech Mater 2013;332.